Journal of Power Sources 233 (2013) 86–92

Contents lists available at SciVerse ScienceDirect

Journal of Power Sources

journal homepage: www.elsevier.com/locate/jpowsour

Carbazole-based molecular glasses for efficient solid-state dye-sensitized solar cells

G. Puckyte [a], B. Schmaltz [b], A. Tomkeviciene [a,d], M. Degbia [b], J.V. Grazulevicius [a,**], H. Melhem [c], J. Bouclé [c], F. Tran-Van [b,*]

[a] Kaunas University of Technology, Department of Organic Technology, Radvilenu pl. 19, LT-50254 Kaunas, Lithuania
[b] Université F. Rabelais, Laboratoire PCM2E, Parc de Grandmont, 37200 Tours, France
[c] Institut XLIM UMR 7252, Université de Limoges/CNRS, 123 av. A. Thomas, 87060 Limoges cedex, France
[d] Vilnius University, Institute of Applied Research, Sauletekio 9-III, LT-10222 Vilnius, Lithuania

HIGHLIGHTS

- Mono- and di-substituted carbazole molecular glasses were synthesized.
- The di-substituted molecule appeared to have better photovoltaic properties.
- Without optimization, the carbazole derivative shows higher J_{sc} than the spiro-OMeTAD.

GRAPHICAL ABSTRACT

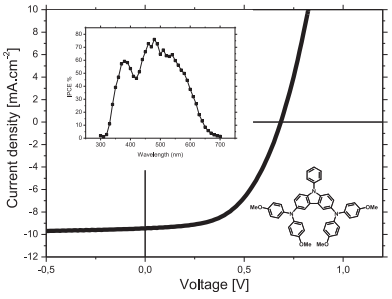

ARTICLE INFO

Article history:
Received 11 July 2012
Received in revised form
15 December 2012
Accepted 21 January 2013
Available online 29 January 2013

Keywords:
Organic photovoltaics
Solid-state dye-sensitized solar cells
Molecular glasses
Organic hole transporting materials

ABSTRACT

Efficient molecular glasses based on carbazole moiety used as hole transporting materials were synthesized. The role of the mono- or di-substitution of dimethoxy-diphenyl amine groups on the 3 and/or 6 position of the carbazole was evidenced. Their thermal, optical, photoelectrical, electrochemical properties as well as their photovoltaic characteristics on solid-state dye sensitized solar cells were investigated. The performance of these materials in solid-state DSSC based on TiO_2 sensitized with the commercial indoline organic dye D102 is widely discussed. In such configuration, a power conversion efficiency of 3.4% and a fill factor of 0.53 are achieved with a 3,6-substitued carbazole molecular glass derivative, under standard AM 1.5 simulated solar irradiation. In addition, the J_{sc} value is even higher than the spiro-OMeTAD, due to its higher mobility. These results are found to be very promising since no specific optimization was performed on the devices yet. By comparison, the corresponding reference device incorporating spiro-OMeTAD as *p*-type organic semiconductor gives similar power conversion efficiency of 3.5%, showing the relevance of our approach.

1. Introduction

During the last two decades, dye-sensitized solar cells (DSSC) attracted the attention of many research worldwide and became the low-cost solar cells with the highest efficiencies exceeding 12% [1–5]. The mechanisms of such devices lie on the photo-induced electron transfer from a dye to the conduction band of a nanostructured oxide (usually titanium dioxide, TiO_2). The dye is

* Corresponding author. Tel.: +33 247366923; fax: +33 247367073.
** Corresponding author. Tel.: +370 7 488941; fax: +370 7 456525.
E-mail addresses: Juozas.Grazulevicius@ktu.lt (J.V. Grazulevicius), francois.tran@univ-tours.fr (F. Tran-Van).

0378-7753/$ – see front matter © 2013 Elsevier B.V. All rights reserved.
http://dx.doi.org/10.1016/j.jpowsour.2013.01.137

then reactivated by a liquid electrolyte containing a redox couple (I_3^-/I^- in acetonitrile). However, the use of a liquid electrolyte is associated with several limitations, such as leakages and corrosion of the electrode materials. That is why a specific sealing technology is required. The liquid electrolyte increases the fabrication cost and makes the device more complex. A strategy which was developed few years ago consists in the fabrication of "solid-state" DSSC (ssDSSC) by replacing the liquid electrolyte by a *p*-type organic semiconductor or a polymer matrix associated with a redox couple. Different low molecular weight compounds such as triphenylamine [6,7], carbazole [8,9] or conjugated polymer like poly(3,4-ethylenedioxythiophene) (PEDOT) or poly-3-hexylthiophene [10] (P3HT) have been suggested. Recently, X. Liu et al. [11] reported the fabrication of indoline D205 dye-sensitized solar cells (DSSCs) with photoelectrochemically polymerized PEDOT as a hole conductor. Under optimized conditions (wavelength of monochromatic light used for the polymerization of PEDOT), the efficiency of ssDSSCs reaches 7.1%. Nowadays, one of the most studied material is the 2,2,7,7-tetrakis-(*N*,*N*-di*p*-methoxyphenylamine)-9,9-spirobifluorene or spiro-OMeTAD, which gives power conversion efficiency over 7% [12–15]. Although intense research efforts are conducted worldwide in order to develop efficient alternatives to spiro-OMeTAD, only few compounds compete with its reported efficiencies [16].

In this paper, we focus on the synthesis and design of new *p*-type organic semiconductor molecular glasses based on carbazole moieties. More attention will be given to the comparison between mono- and di-functionalized (4,4′-dimethoxydiphenylaminyl)-9-phenylcarbazole in position 3 and/or 6, and the state-of-the-art spiroOMeTAD. Their thermal and electronic properties will be described. The performance of these materials in solid-state DSSC based on TiO_2 sensitized with the commercial indoline D102 organic dye will be widely discussed.

2. Material and methods

2.1. Materials

4,4-dimethoxydiphenylamine, potassium carbonate, copper powder, 18-crown-6 and 1,2-dichlorobenzene, acetylacetone were purchased from Sigma Aldrich, Alfa Aesar, Fluka and used as received. Titanium (IV) isopropoxide (97%), Lithium Bis(trifluoromethanesulfonyl)imide salt, Titanium tétrachloride, 4-tert-butylpyridine, acetonitrile, terbutanol, chlorobenzene and ethanol were purchased from Aldrich Sigma. D102 dye was received from Mitsubishi Paper Mills. TiO_2 paste (18NR-T) was purchased from Dyesol. 2,2,7,7-tetrakis-(*N*,*N*-di*p*-methoxyphenylamine)-9,9-spirobifluorene was received from Merk Kga. Fluorine-doped SnO_2 conducting glass (TCO2215, 15 Ω sq^{-1}) was purchased from Solaronix.

2.2. Instruments and measurements

^1H and ^{13}C NMR spectra were recorded using Varrian Unity Inova [300 MHz (^1H), 75.4 MHz (^{13}C)] spectrometer at room temperature. All the data are given as chemical shifts in δ (ppm), $(CH_3)_4Si$ (TMS, 0 ppm) was used as an internal standard. Elemental analysis was performed with an Exeter Analytical CE-440 Elemental. Mass (MS) spectra were recorded on a Waters ZQ (Waters, Milford, MA). Differential Scanning Calorimetry (DSC) measurements were carried out using Perkin–Elmer DSC-7 series thermal analyzer at a heating rate 10 °C min^{-1} under nitrogen flow. Thermogravometric analysis (TGA) measurements were performed on a Mettler Toledo TGA/SDTA 851[e]. The UV–Vis spectra were recorded as dilute solutions of the synthesized compounds in THF on Perkin Elmer Lambda 35 spectrophotometer. A microcell with an internal width of 1 mm and 10^{-5} M solution of investigated materials was used. Fluorescence spectra of the sample in THF (10^{-5} M) were recorded with a Hitachi MPF-4 spectrometer. Cyclic voltammetry of the carbazole derivatives was performed in a 10^{-3} mol L^{-1} acetonitrile solution with 0.1 mol L^{-1} of tetraethylammonium tetrafluoroborate ($TEABF_4$) as supporting electrolyte at scan rate of 50 mV s^{-1}. Platinum wire and disk (1 cm diameter) electrodes were used as counter and working electrodes, respectively. Silver wire was used as a pseudo-reference electrode. At the end of the measurements, ferrocene has been added as internal reference.

The ionization energy (EI) of the synthesized compounds was measured on thin films by electron photoemission in air. The samples were prepared by dissolving materials in THF and were coated on Al plates pre-coated with ~0.5 μm thick methylmethacrylate and methacrylic acid copolymer adhesive layer. The thickness of the transporting material layer was 0.5–1 μm.

The samples for the hole mobility measurements were prepared by spin-coating solutions of the synthesized compounds on polyester films with conductive Al layer. The layer thickness was in the range 5–10 μm. The hole drift mobility was measured by xerographic time of flight technique (XTOF) [17,18]. The electric field was created by positive corona charging. The charge carriers were generated at the layer surface by a pulsed nitrogen laser (pulse duration of 2 ns, wavelength of 337 nm). The layer surface potential decrease as a result of pulse illumination, within 1–5% with regard to the initial potential before illumination. The capacitance probe that was connected to the wide frequency band electrometer measured the speed of the surface potential decrease dU/dt. The transit time t_t was determined by the kink on the curve of the dU/dt transient in double logarithmic scale. The drift mobility was calculated by the formula $\mu = d^2/U_0 t_t$, where d is the layer thickness, U_0 the surface potential under illumination.

Transient photovoltage and photocurrent decay measurements were performed on complete working solar cells in order to probe the charge kinetics under different illumination conditions using an experimental setup described elsewhere [19,20]. The incident white illumination, provided by OSRAM LEDs, varied up to approximately 80 mW cm^{-2} on the devices, in order to probe the intrinsic charge kinetics under realistic working conditions. For each light intensities, the short-circuit current density and open-circuit voltage of the devices was measured, before an additional light pulse, provided by a green LED (550 nm) controlled by a solid-state switch, was applied. The pulse power density was adjusted in order to be less than 3% of the steady-state white illumination for all illumination conditions, so that a first order perturbation regime was ensured. The device transient responses were recorded under open-circuit and short-circuit conditions in order to extract the recombination and charge extraction decay times respectively. In both cases, the transient signals were fitted using mono-exponential functions from which the decay times were extracted.

2.3. Synthesis of materials

All reactions were carried out under a nitrogen atmosphere.

The synthesis of 3-(4,4′-dimethoxydiphenylaminyl)-9-phenylcarbazole (**2a**) has already been described in the literature [21].

3,6-Di(4,4′-dimethoxydiphenylaminyl)-9-phenylcarbazole (**2b**) was prepared from 3,6-diiodo-9-phenylcarbazole (2.4 g, 4.8 mmol), 4,4′-dimethoxydiphenylamine (3.3 g, 14.4 mmol), 18-crown-6 (0.06 g, 0.2 mmol), potassium carbonate (5.3 g, 38.4 mmol) and copper powder (1.22 g, 19.2 mmol) were refluxed in *o*-dichlorobenzene (5 ml) under argon for 24 h. Then copper and inorganic salts were removed by filtration of the host reaction mixture. The solvent was distilled under reduced pressure. The product was

purified by column chromatography with silica gel using hexane/acetone (3/1) as eluent to give yellow powder.

Yield: 60% (2.03 g).

^1H *NMR* (300 *MHz*, *CDCl*$_3$, *δ*, *ppm*): 3.81 (12 H, s, OMe), 6.78–7.42 (23 H, m, Ar), 7.50 (2 H, d, $J = 8.8$ Hz, Ar), 7.82 (2 H, s, Ar).

^{13}C *NMR* (75.4 *MHz*, *CDCl*$_3$, *δ*, *ppm*): 55.8 (OMe), 110.8, 111.0, 114.2, 119.3, 122.8, 124.2, 124.7, 125.0, 127.5, 130.1, 130.6, 140.6, 141.6, 152.6.

MS (*APCl*$^+$, 25 *V*) *m*/*z*: 698 ([M + H]$^+$, 96%).

Elemental analysis. Calcd. for $C_{46}H_{39}N_3O_4$ (%): C 79.17, H 5.63, N 6.02; found (%): C 78.89, H 5.80, N 6.14.

2.4. Photovoltaic device fabrication and characterization

FTO/TiO_2/dye films were prepared as described below. The F-doped SnO_2 (FTO) glass substrates are subsequently sonicated for 10 min in acetone, isopropanol and water, before being treated for 10 min by UV–ozone treatment. A compact layer of TiO_2 is deposited by spray-pyrolysis [22] at 450 °C from a solution of titanium isopropoxyde and acetylaceton in ethanol (Sigma–Aldrich). The layers are then annealed at 450 °C for 20 min. A nanoporous layer of TiO_2 is applied by spin coating from a commercial TiO_2 paste (DSL 18NRT, Dyesol) containing nano-sized anatase particles, followed by gradual annealing from 250 °C up to 500 °C, over 30 min. The resulting film thickness (2–2.5 μm) is a good compromise for solid-state DSSC, resulting in balanced light absorption and charge collection.

The substrates are then treated in a 0.02 M $TiCl_4$ aqueous solution for 2 h [23,24] and rinsed with water followed by annealing at 500 °C for 45 min. Subsequently, they are sensitized by soaking in 0.6 mM solution of indoline D102 dye (Mitsubishi Paper Mills) in Acetonitrile:Ter-butanol (1:1 vol%) (Sigma–Aldrich) overnight at 80 °C and then washed with acetonitrile. The hole conductor layer is deposited by spin coating from a solution of the monomer **2b** in chlorobenzene (Sigma–Aldrich) at 200 mg mL^{-1}, containing Li(CF$_3$SO$_2$)$_2$N solution (190 mg mL^{-1}) in acetonitrile with ratio of Li(CF$_3$SO$_2$)$_2$N:monomer (1:27 vol%) and ter-butylpyridine (1:57 vol %) (Sigma–Aldrich). Before spin coating, the solution deposited onto the dye sensitized substrates was allowed to fill TiO_2 pores for 40 s. Gold top electrodes were finally evaporated under vacuum (10^{-6} mbar) using shadow masks that define two active areas per substrates (0.18 cm^2 each).

The Current density–voltage (*J*–*V*) characteristics were recorded in air using a Keithley 2400 source-measure unit, in the dark and under simulated solar emission (Atlas Solarconstant 575PV). The spectral mismatch between the emission of the solar simulator and the global AM1.5G solar spectrum (ASTM G173-03) was corrected using a mismatch factor [25] and the solar simulator irradiance was adjusted accordingly using a certified silicon reference cell in order to achieve an equivalent AM1.5G irradiance of one sun (100 mW cm^{-2}) on the test cells.

3. Results and discussion

3.1. Synthesis

The facile synthetic route of the 3-(4,4′-dimethoxydiphenylaminyl)-9-phenylcarbazole and 3,6-di(4,4′-dimethoxydiphenylaminyl)-9-phenylcarbazole (**2a** and **2b**) is shown on Fig. 1. Both molecules were synthesized through a one-step reaction from mono- (**1a**) and diiodo-9-phenylcarbazole (**1b**) with respectively yields between 60 and 70%. According to Ullmann reaction, the iodo-derivatives were reacted with copper, potassium carbonate and 18-crown-6 in *o*-dichlorobenzene to form the yellow desired products, which were purified by column chromatography.

The design of **2a** and **2b** has been thought to fulfill several conditions. In order to improve the solubility of the hole transporting material (HTM) as well as to keep their molecular glass behavior and to increase the hole mobility, dimethoxy-diphenylamine groups have been introduced to the most reactive 3- and 6-positions of the carbazole moiety. As mentioned previously, the molecular glass properties of the HTM is important to ensure an efficient filling of the pores of the TiO_2 and so a better contact area between the TiO_2 and the HTM [5]. Furthermore, a phenyl group has been introduced on the 9-position of the carbazole, allowing to keep higher glass transition temperature compare to alkyl groups [8]. In addition, the phenyl moiety on the 9-position has another crucial role since it has a positive effect on the mobility of the HTM compared to the ethyl groups [26].

3.2. Photophysical properties

Molecule **2b** and its mono-substituted analogous **2a** are well soluble in common organic solvents, such as toluene, tetrahydrofuran (THF), dichloromethane, and chloroform. The optical absorption and fluorescence (Fig. 2) spectra in THF were measured at a concentration of ca. 10^{-5} M. The wavelengths (λ) of the maximum absorption peak of the carbazole derivatives are summarized in Table 1. In solution, **2b** exhibits two absorption peaks at 330 nm corresponding to the π–π* absorption of conjugated molecule and a peak, weak in intensity, at 398 nm. Knowing that the absorption spectrum of spiroMeOTAD exhibit also two absorption peaks at 310 and 390 nm [27], we can expect similar optical properties for the 9-phenyl-3,6-(di-*p*-methoxyphenylamine)-carbazole. In the literature [28], the maximum of absorption of the dye D102, used as sensitizer, is 501 nm. We can say that the molecular glass will not interfere with the absorption of the dye, allowing efficient generation of charge carriers via the sensitizer. The optical bandgap (E_g^{opt}) of **2b**, calculated from the absorption edges on the UV–Vis spectrum of the solution, was 2.85 eV, which is smaller than the mono-substituted analogous **2a** (0.1 eV). The bandgap of **2b** is also slightly smaller than the bandgap of the spiroMeOTAD (2.98 eV) [8]. The extinction coefficient was measured and given 1.2×10^5 M^{-1} cm^{-1}, which is higher than the ssDSSCs HTM spiroMeOTAD reference (0.7×10^5 M^{-1} cm^{-1}) [27].

3.3. Thermal properties

The thermal properties of the two HTM were estimated by DSC and TGA (Table 2). Both molecules show high thermal stability as demonstrated by their high values of T_{ID} (5% weight loss temperature). Compounds **2a** and **2b** exhibit respectively a T_{ID} of 388 °C and 441 °C. Even if the disubstituted carbazole based derivative **2b** shows higher glass transition temperature than the mono-substituted molecule, they both demonstrate molecular glass behavior. Although molecule **2a** was obtained as crystalline material, it formed glasses by cooling down the melted sample (after the first cycle). On the contrary, molecule **2b** was isolated as an amorphous material. No change was observed after several melting/cooling cycles. It can be noticed that the T_g of compound **2b** is slightly lower than the one of the standard hole transporting material (i.e. sipo-OMeTAD) given for 120 °C [12]. The ability of such low molar mass materials to stay amorphous in a metastable state allows the realization of good contacts between the thin films and the nanostructured TiO_2 layer [12].

3.4. Electrochemical properties

Electrochemical cyclic voltammetry has been widely employed to investigate the redox behavior of conjugated molecules and to estimate HOMO and LUMO energy levels. The cyclic

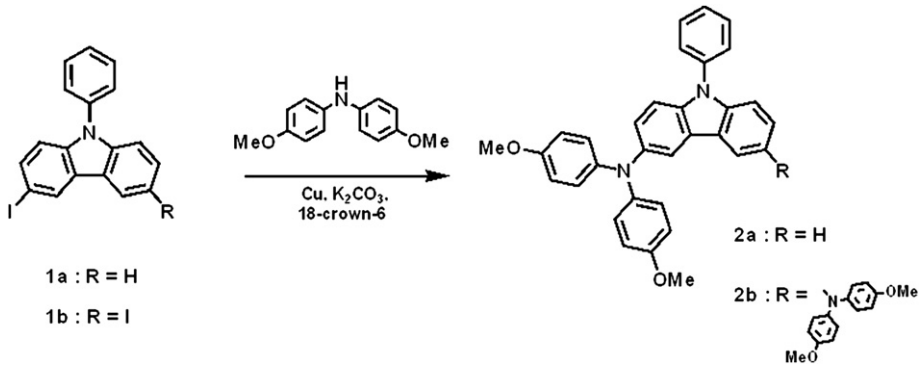

Fig. 1. Synthetic scheme for the preparation of HTM **2a** and **2b**.

voltammagrams of **2a** and **2b** are shown on Fig. 3. On the anodic sweep, **2b** showed two reversible one electron oxidations with half wave potentials of 0.15 V and 0.33 V respectively (vs. Fc/Fc^+). These two reversible oxidation potentials correspond to the formation of radical cation of the carbazole moiety and the dication quinonediimine, respectively [29]. Concerning molecule **2a**, the anodic sweep showed one reversible one electron oxidation with half wave potentials of 0.32 V vs. Fc/Fc^+. **2a**, which has an open reactive 6-position, exhibit stable redox properties since the formation of radical cations in the solution didn't lead to the creation of dimer of the carbazole derivatives as usually observed for 3-monosubstituted carbazole [30]. It means that the 3-subtituted diphenylamine stabilize the radical cation and should ensure a stable device after filling the material inside the mesoporous sensitized TiO_2.

From the half wave oxidation potential ($E_{1/2,ox}$) of the semiconductor, HOMO energy level has been calculated according to the following equations [31]: HOMO (eV) $= -e(E_{1/2,ox} + 4.8)$ where $E_{1/2,ox}$ is the half measured difference of potential between the oxidation and the reduction on the first wave relative to Fc/Fc^+. The results of the electrochemical measurements and calculated HOMO energy levels as well as the deduced LUMO energy level (from UV/Vis absorption spectrum) of the molecules are listed in Table 3. The estimated HOMO/LUMO energy levels of **2a** and **2b** are −4.95/−2.10 eV and −5.12/−2.17 eV, respectively (Table 3). These values are in good agreement with the increase of the donor character of **2b** resulting into an increase of the HOMO level. Compared to spiro-OMeTAD, the most promising molecule **2b** has similar HOMO (−4.95 vs. −5.03 eV [8]) and LUMO levels (−2.10 vs. −2.05 eV).

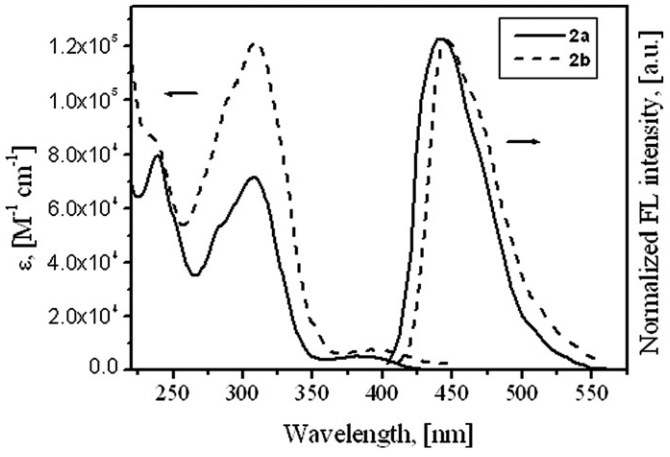

Fig. 2. UV/Vis absorption and fluorescence (λ_{ex} = 330 nm) spectra of the dilute THF solutions (10^{-5} M) of the compounds **2a** and **2b**.

3.5. Photoelectrical properties

The ionization energy was measured by photoemission in air method from films. The HOMO energy level of **2a** and **2b** are presented in Table 3. The calculated values confirm the results from cyclic voltammetry since **2b** seems to have a higher HOMO level (5.04 eV). These differences are apparently due to the differences in molecular interactions and molecular arrangements in thin solid layers and in dilute solutions of these derivatives and also due to the difference between dynamic vs. static methods. However, these results approve the similar HOMO energy level between **2b** and spiro-OMeTAD (5.11 eV determined by photoelectron spectroscopy) [8]. Since HOMO levels vary only ±0.1 eV from spiro-OMeTAD, hole injection from the dye to the HTM should be similar.

After injection, holes must be efficiently transported to the cathode. That is the reason why the mobility of these new HTM was measured by the xerographic time-of-flight (XTOF) technique. At room temperature, μ showed linear dependencies on the square root of the electric field. Hole drift mobility values of the amorphous film of **2b** was 3.3×10^{-3} cm^2 V^{-1} s under an electric field of 6.4×10^5 V cm^{-1} which is ten times higher than the monosubstituted derivative (4.4×10^{-4} cm^2 V^{-1} s for **2a** [21]). By comparison, hole mobility of Spiro-OMeTAD, measured by time-of-flight, is 2×10^{-4} cm^2 V^{-1} s [32].

It should be noted that the measurements have been obtained on pure HTM films that is to say without addition of lithium bis(trifluoromethylsulfonyl)imide salt (Li-TFSI) which is expected to increase the mobility of the charge carrier [33]. So, we can expect a better mobility of the holes in the HTM when integrated into the solar cell device. On the other hand, the higher mobility for **2b** could also be admitted to the design of the molecule, with the introduction of the phenyl group on the 9-position of the carbazole [26].

3.6. Photovoltaic properties

Photovoltaic properties of **2a**/**2b** were investigated by fabricating solid-state dye-sensitizer solar cells with (5-{1,2,3,3a,4,8b-hexahydro-4-[4-(2,2-diphenylvinyl)phenyl]-cyclopeanta[b]indole-7-ylmethylene}-4-oxo-2-thioxo-thiazolidin-3-yl)acitic acid (D102) dye and **2a**/**2b** as *p*-type semiconductor material. In order to compare the properties, cells with spiro-OMeTAD as *p*-type

Table 1
Absorption and emission characteristics of compounds **2a**–**b**.

Compound	UV, λ_{onset}, [nm]	E_g^{opt}[a], [eV]	FL, λ_{max}, [nm]
2a	420	2.95	440
2b	435	2.85	446

[a] The optical band gaps E_g^{opt} estimated from the edges of electronic absorption spectra.

Table 2
Thermal characteristic of compounds **2a**–**b**.

Compound	**2a**	**2b**
T_g[a], [°C]	65	97
T_m[a], [°C]	145[c]	–
T_{ID}[b], [°C]	388	441

[a] Determined by DSC, scan rate 10 °C min^{-1}, N_2 atmosphere.
[b] 5% weight loss determined by TGA, heating rate 10 °C min^{-1}, N_2 atmosphere.
[c] 1st heating only.

material have been used as reference. The device structure is FTO/TiO_2/D102/hole transporter/Au. The corresponding photovoltaic parameters are summarized in Table 4. The hole transporting layer (HTL) was spin-coated from chlorobenzene solution (200 mg mL^{-1}) at room temperature. The current density–voltage (J–V) characteristics of the device in the dark and under the illumination of AM 1.5, 100 mW cm^{-2} are shown on Fig. 4a.

The device built with hole transporter **2a** [21] give low J_{sc} value (2.63 mA cm^{-2}) leading to a low power conversion efficiency (PCE) of 0.54%. On the opposite, the devices fabricated from the **2b** compound exhibit high J_{sc} values (9.47 mA cm^{-2}) that are found to be over that of cell based on spiro-OMeTAD (7.18 mA cm^{-2}) under the same preparation conditions, showing the necessity of the difunctionalization of the 3,6-carbazole.

These observations are consistent with the IPCE measured for the corresponding cells, which are not optimized devices. Indeed, J_{sc} values for reference devices based on D102 and spiro-OMeTAD are usually found around 8–9 mA cm^{-2} [20], leading to IPCE of over 60% at 500 nm. In the case of our study based on non-optimized devices, the hole mobility of compounds **2b** is found to be in the order of 10^{-3} cm^2 V^{-1} s^{-1}. This order of magnitude is compatible with mobility values measured for spiro-OMeTAD and for conventional molecular glasses [32,33]. Typically, a gain of one order of magnitude in hole mobility can lead to substantial increase in device performance, as it was already observed for spiro-OMeTAD using lithium salt dopants and tert-butylpyridine, although other effects are also induced by these additions [34,35]. In these studies, a gain of up to 50% in J_{sc} is demonstrated. In a related study, the hole mobility of spiro-OMeTAD was drastically improved by one to two orders of magnitude, using dopants based on cobalt, leading to a gain of around 10–20% in J_{sc} as well [15]. Considering these elements and considering the fact that similar dye-sensitized electrodes are used for all devices so that the amount of dye molecule grafted on TiO_2 is similar, it is reasonable to consider that the gain in mobility for

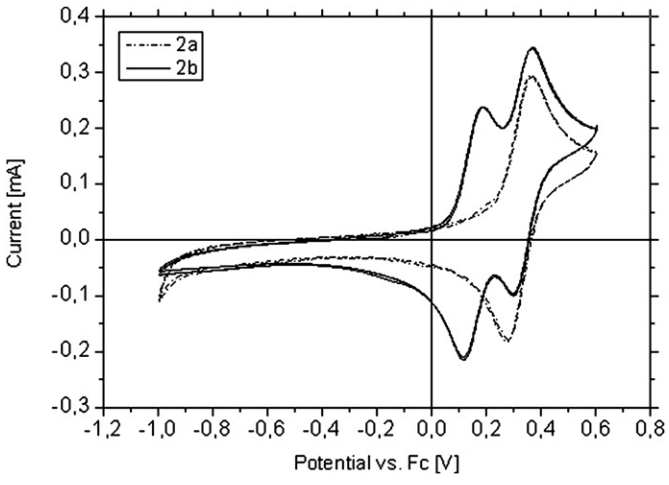

Fig. 3. Cyclic voltammetry of **2a** and **2b** in acetonitrile (10^{-3} M) with 0.1 M of $N(Et)_4BF_4$ Work electrode: Pt, V = 50 mV S^{-1}.

Table 3
HOMO, LUMO, and electrochemical characteristics of **2a**–**b**.

Compound	$E_{1/2}$, [V]	E_I[a], [eV]	E_{HOMO}[b], [eV]	E_{LUMO}[c], [eV]
2a	0.33	5.10	−5.12	−2.17
2b	0.15	5.04	−4.95	−2.10

[a] Ionization energy was measured by the photoemission in air method from films.
[b] $E_{HOMO} = -4.8 + E_{1/2}$.
[c] $E_{LUMO} = E_{HOMO} - E_g^{opt}$.

compound **2b** can explain the larger photo-current observed with regard to the cell based on spiro-OMeTAD.

In order to confirm the results, three batches have been done under the same conditions. All the batches gave higher J_{sc} value for molecule **2b** than the spiro-OMeTAD, which can be explained by the higher mobility of **2b** compared with the reference.

As shown from the J–V measurement in the dark (Fig. 4a), the **2b** turn on-voltage is lower than that of Spiro-OMeTAD. This indicates that the film of **2b** in the device is less resistive than the one containing Spiro-OMeTAD. These results are in good agreement with a higher mobility of the thin layer of 2b vs. Spiro-OMeTAD as already discussed from the J_{sc} values.

The optimal D102:**2b** device exhibited PCE of 3.44% with a V_{oc} of 0.69 V and a fill factor of 53%. To the best of our knowledge, this PCE value is among the highest reported to date for small-molecule p-type semiconductor materials other than spiro-OMeTAD [36–41]. Furthermore, by comparison to the PCE of the spiro-OMeTAD device, the results obtained with **2b** are similar and are very encouraging since the devices have been built without any optimizations. In particular, the V_{oc} value can be increased by optimization of the pore filling or the concentration of the hole transporting material solution [42]. Usually, device optimization with spiro-OMeTAD/D102 system leads to PCE over 4%. The obtained results here suggest that the compound **2b** is very promising to achieve highly efficient solid-state DSSC.

Fig. 4b shows the external quantum efficiency (EQE) spectra of the solid-state DSSC [FTO/TiO_2/D102/**2b**/Au] under the monochromatic illumination (current density–voltage and EQE spectra of [FTO/TiO_2/D102/**2b**/Au] is shown in ESI). The device shows a broad response range from 300 to 670 nm. High IPCE values over 50% are reached in the 370–580 nm range and a maximum IPCE of almost 75% is reached around 480 nm. This value is very high compared to state of the art devices based on D102, and is compatible with the high photo-current evidenced for this device. The value of J_{sc} obtained through integration of this IPCE (8.63 mA cm^{-2}) was in reasonable agreement with that measured from the J–V curve (9.45 mA cm^{-2}). By comparison to the Spiro-OMeTAD cell, the device containing **2b** shows higher IPCE values (+50%) in the 370–580 nm range, confirming the promising interest to this HTM.

The large differences in IPCE for both devices is magnified as IPCE are estimated under low light intensities regime (μW cm^{-2}), for which larger charge lifetimes have been evidenced by transient photovoltage decay measurements (see below) for compound **2b** compared to device based on spiro-OMeTAD.

Transient photovoltage and photocurrent decay measurements were performed to better interpret the photovoltaic performance of the devices. In particular, recombination kinetics are estimated

Table 4
Photovoltaic parameters of the solid-state DSSC under illumination.

Composition	J_{sc} [mA cm^{-2}]	V_{oc} [mV]	FF [%]	Eff. [%]
TiO_2/D102/**spiro**/Au	7.18	860	57	3.53
TiO_2/D102/**2a**/Au	2.63	630	32	0.54
TiO_2/D102/**2b**/Au	9.47	690	53	3.44

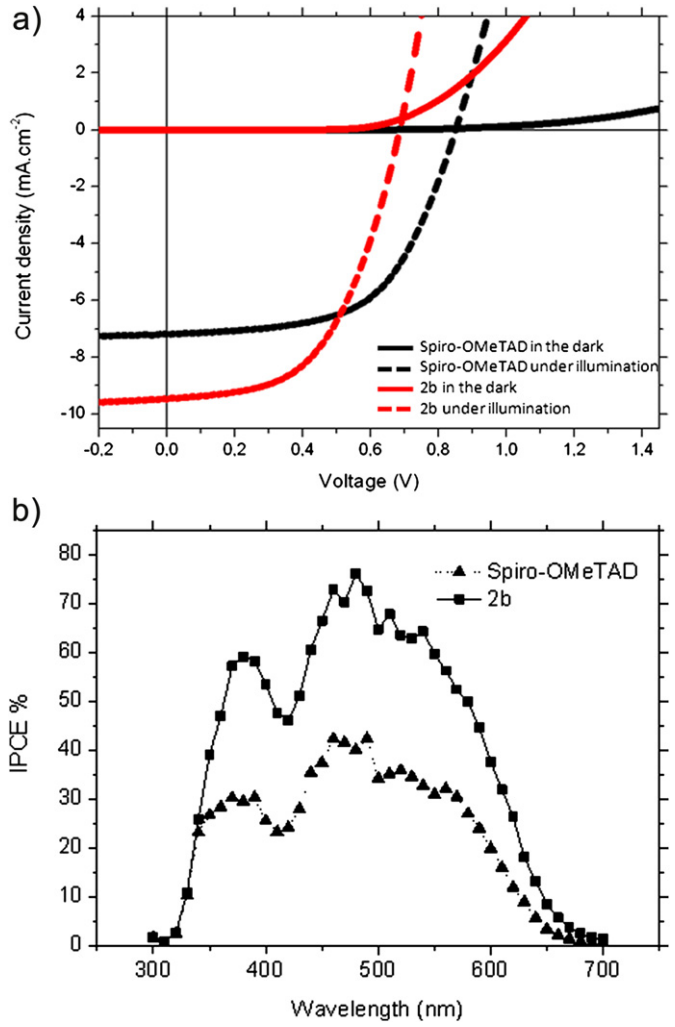

Fig. 4. a) Current density–voltage curves in the dark (dash lines) and under illumination (solid lines) of the devices with D102 as sensitizer and spiro-OMeTAD (black) and **2b** (red) as HTM; b) incident-photon-to-current conversion efficiency (IPCE) of devices with spiro-OMeTAD (triangles) and **2b** (squares). (For interpretation of the references to color in this figure legend, the reader is referred to the web version of this article.)

under open-circuit condition, and charge extraction kinetics are probed under short-circuit conditions (see experimental details) for solar cells based on spiro-OMeTAD and compound **2b** respectively (this choice is driven by device performance, which are quite close for both cells). The corresponding decay times are plotted in Fig. 5. These measurements help to better interpret the observed photovoltaic parameters. In particular, while both devices exhibit similar charge extraction kinetics – hence quite comparable charge transport properties – over the entire illumination range, charge recombination times show different evolutions as a function of incident light intensities. Recombination is found to be slightly slower at low light intensities for device based on compound **2b** compared to spiro-OMeTAD. However, under higher illumination intensities up to 80 mW cm^{-2} (highest achievable power density considering our experimental set-up), recombination is found to be faster. Especially, a simple extrapolation up to standard illumination conditions (100 mW cm^{-2}) lead to a faster charge recombination for device based on compounds **2b** than that of spiro-OMeTAD. A faster charge recombination for compound **2b** is consistent with the reduced open-circuit voltage observed in the *J*(*V*) characteristics under full sun for this device compared to spiro-

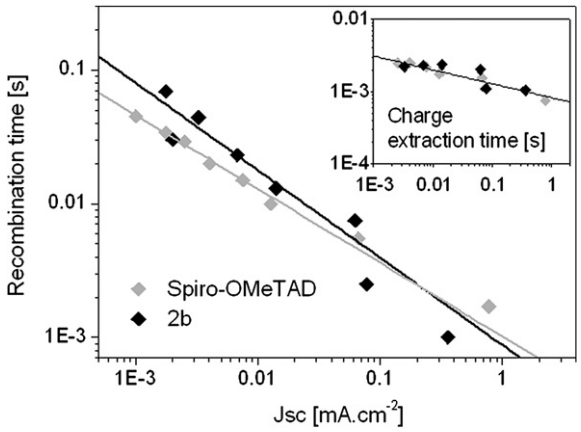

Fig. 5. Recombination time and (in insert) charge extraction time under short circuit conditions for **2b** (dark squares) and spiro-OMeTAD (gray squares).

OMeTAD. Moreover, the different slopes evidenced for both devices indicate that slightly different recombination mechanisms are occurring. Recombination kinetics is known to be affected by the energetic configuration at the interface, as well as by the intimate chemical interactions of the hole transporter and the dye. In our case, compound **2b** shows a higher hole mobility compared to spiro-OMeTAD, and a limited charge extraction cannot explain the slightly faster recombination observed. Both spiro-OMeTAD and compound **2b** exhibit methoxy groups, as well as comparable frontier orbitals. Our transient data suggest that some slight changes in the local configuration of the molecular glass with regard to the D102 dye can be at the origin of additional recombination in the case of compounds **2b**. Further investigations would be required in order to address this issue.

4. Conclusion

In summary, we have synthesized and characterized new hole transporting materials based on carbazole moiety and substituted with one or two bis-(4-methoxy-phenyl)-amine groups on the 3 and/or 6 position of the carbazole for application in solid-state DSSC. We demonstrate that the di-functionalized molecular glass **2b** exhibit better properties than the mono-functionalized in terms of glass transition temperature, mobility and appropriate energy level. We emphasized the similar photovoltaic performances of **2b** compared to the well-known reference hole transporter material (HTM) spiro-OMeTAD. In particular, without any device optimization, a power conversion efficiency of 3.44% is achieved with this new HTM with a J_{sc} of 9.47 mA cm^{-2}, which is found to be higher than that of the reference device based on spiro-OMeTAD. This result shows the strong potentialities of this compound for hybrid photovoltaic energy conversion.

Acknowledgments

This research was funded by a grant (No MIP-059/2011) from the Research Council of Lithuania and the Region Centre. A. Tomkeviciene acknowledges European Union Structural Funds project “Postdoctoral Fellowship Implementation in Lithuania” for funding herpostdoctoral fellowship.

Appendix A. Supplementary data

Supplementary data related to this article can be found at http://dx.doi.org/10.1016/j.jpowsour.2013.01.137.

References

[1] A. Yella, H.-W. Lee, H.N. Tsao, C. Yi, A.K. Chandiran, M.K. Nazeeruddin, E.W.-G. Diau, C.-Y. Yeh, S.M. Zakeeruddin, M. Grätzel, Science 334 (2011) 629–634.
[2] Y. Chiba, A. Islam, Y. Watanabe, R. Komiya, N. Koide, L. Han, Japanese Journal of Applied Physics 45 (2006) L638–L640.
[3] Z.-S. Wang, T. Yamaguchi, H. Sugihara, H. Arakawa, Langmuir 21 (2005) 4272–4276.
[4] M.A. Green, K. Emery, Y. Hishikawa, W. Warta, Progress in Photovoltaics Research and Applications 18 (2010) 346–352.
[5] W.-S. Jeong, J.-W. Lee, S. Jung, J.H. Yun, N.-G. Park, Solar Energy Materials and Solar Cells 95 (2011) 3419–3423.
[6] D.P. Hagberg, J.-H. Yum, H. Lee, F. De Angelis, T. Marinado, K.M. Karlsson, R. Humphry-Baker, L. Sun, A. Hagfeldt, M. Grätzel, M.K. Nazeeruddin, Journal of the American Chemical Society 130 (2008) 6259–6266.
[7] E.L. Unger, E. Ripaud, P. Leriche, A. Cravino, J. Roncali, E.M.J. Johansson, A. Hagfeldt, G. Boschloo, The Journal of Physical Chemistry C 114 (2010) 11659–11664.
[8] T. Leijtens, I.K. Ding, T. Giovenzana, J.T. Bloking, M.D. McGehee, A. Sellinger, ACS Nano 6 (2012) 1455–1462.
[9] R.-H. Lee, T.-F. Cheng, J.-W. Chang, J.-H. Ho, Colloid & Polymer Science 289 (2011) 817–829.
[10] R. Zhu, C.-Y. Jiang, B. Liu, S. Ramakrishna, Advanced Materials 21 (2009) 994–1000.
[11] X. Liu, Y. Cheng, L. Wang, L. Cai, B. Liu, Physical Chemistry Chemical Physics 14 (2012) 7098–7103.
[12] U. Bach, D. Lupo, P. Comte, J.E. Moser, F. Weissortel, J. Salbeck, H. Spreitzer, M. Grätzel, Nature 395 (1998) 583–585.
[13] N. Cai, S.-J. Moon, L. Cevey-Ha, T. Moehl, R. Humphry-Baker, P. Wang, S.M. Zakeeruddin, M. Grätzel, Nano Letters 11 (2011) 1452–1456.
[14] J. Bouclé, J. Ackermann, Polymer International 61 (2011) 355–373.
[15] J. Burschka, A. Dualeh, F. Kessler, E. Baranoff, N.-L. Cevey-Ha, C. Yi, M.K. Nazeeruddin, M. Grätzel, Journal of the American Chemical Society 133 (2011) 18042–18045.
[16] J. Kim, J.K. Koh, B. Kim, S.H. Ahn, H. Ahn, D.Y. Ryu, J.H. Kim, E. Kim, Advanced Functional Materials 21 (2011) 4633–4639.
[17] E. Montrimas, V. Gaidelis, A. Pazera, Lithuanian Journal of Physics 6 (1966) 569.
[18] S.M. Vaezi-Nejad, International Journal of Electronics 62 (1987) 361.
[19] B.C. O'Regan, F. Lenzmann, The Journal of Physical Chemistry B 108 (2004) 4342–4350.
[20] H. Melhem, P. Simon, L. Beouch, F. Goubard, M. Boucharef, C. Di Bin, Y. Leconte, B. Ratier, N. Herlin-Boime, J. Bouclé, Advanced Energy Materials 1 (2011) 908–916.
[21] A. Tomkeviciene, G. Puckyte, J.V. Grazulevicius, M. Degbia, F. Tran-Van, B. Schmaltz, V. Jankauskas, J. Bouclé, Synthetic Metals 162 (2012) 1997–2004.
[22] L. Kavan, M. Grätzel, Electrochimica Acta 40 (1995) 643–652.
[23] H.J. Snaith, L. Schmidt-Mende, M. Grätzel, M. Chiesa, Physical Review B 74 (2006) 045306.
[24] L. Vesce, R. Riccitelli, G. Soscia, T.M. Brown, A. Di Carlo, A. Reale, Journal of Non-Crystalline Solids 356 (2010) 1958–1961.
[25] J.M. Kroon, M.M. Wienk, W.J.H. Verhees, J.C. Hummelen, Thin Solid Films 403-404 (2002) 223–228.
[26] A. Sakalyte, J. Simokaitiene, A. Tomkeviciene, J. Keruckas, G. Buika, J.V. Grazulevicius, V. Jankauskas, C.-P. Hsu, C.-H. Yang, The Journal of Physical Chemistry C 115 (2011) 4856–4862.
[27] U. Bach, PhD, 2000.
[28] L. Schmidt-Mende, U. Bach, R. Humphry-Baker, T. Horiuchi, H. Miura, S. Ito, S. Uchida, M. Grätzel, Advanced Materials 17 (2005) 813–815.
[29] J.F. Ambrose, L.L. Carpenter, R.F. Nelson, Journal of the Electrochemical Society 122 (1975) 876–894.
[30] T.X. Lav, F. Tran-Van, F. Vidal, S. Péralta, C. Chevrot, D. Teyssié, J.V. Grazulevicius, V. Getautis, H. Derbal, J.M. Nunzi, Thin Solid Films 516 (2008) 7223–7229.
[31] M. Thelakkat, J. Ostrauskaite, A. Leopold, R. Bausinger, D. Haarer, Chemical Physics 285 (2002) 133–147.
[32] D. Poplavskyy, J. Nelson, Journal of Applied Physics 93 (2003) 341.
[33] H.J. Snaith, M. Grätzel, Applied Physics Letters 89 (2006) 2621114–2621116.
[34] J. Krüger, R. Plass, L. Cevey, M. Piccirelli, M. Grätzel, U. Bach, Applied Physics Letters 79 (2001) 2085–2087.
[35] H.J. Snaith, M. Grätzel, Advanced Materials 19 (2007) 3643–3647.
[36] J.E. Kroeze, N. Hirata, L. Schmidt-Mende, C. Orizu, S.D. Ogier, K. Carr, M. Grätzel, J.R. Durrant, Advanced Functional Materials 16 (2006) 1832–1838.
[37] B. Li, L. Wang, B. Kang, P. Wang, Y. Qiu, Solar Energy Materials and Solar Cells 90 (2006) 549–573.
[38] S. Yanagida, Y. Yu, K. Manseki, Accounts of Chemical Research 42 (2009) 1827–1838.
[39] H.J. Snaith, S.M. Zakeeruddin, Q. Wang, P. Pechy, M. Grätzel, Nano Letters 6 (2006) 2000–2003.
[40] Y. Zhao, W. Chen, J. Zhai, X. Sheng, Q. He, T. Wei, F. Bai, L. Jiang, D. Zhu, Chemical Physics Letters 445 (2007) 259–264.
[41] E.M.J. Johansson, P.G. Karlsson, M. Hedlund, D. Ryan, H. Siegbahn, H.k. Rensmo, Chemistry of Materials 19 (2007) 2071–2078.
[42] I.K. Ding, N. Tétreault, J. Brillet, B.E. Hardin, E.H. Smith, S.J. Rosenthal, F. Sauvage, M. Grätzel, M.D. McGehee, Advanced Functional Materials 19 (2009) 2431–2436.